Protostellar Chimney Flues: Are Jets and Outflows Lifting Submillimeter Dust Grains from Disks into Envelopes?

L. Cacciapuoti[1,2,3] , L. Testi[3,4], L. Podio[3] , C. Codella[3,5] , A. J. Maury[6] , M. De Simone[1,3] , P. Hennebelle[6] ,
U. Lebreuilly[6] , R. S. Klessen[7,8] , and S. Molinari[9]

[1] European Southern Observatory, Karl-Schwarzschild-Straße 2, D-85748 Garching bei München, Germany; luca.cacciapuoti@eso.org
[2] Fakultat für Physik, Ludwig-Maximilians-Universität München, Scheinerstraße 1, D-81679 München, Germany
[3] INAF, Osservatorio Astrofisico di Arcetri, Largo E. Fermi 5, I-50125, Firenze, Italy
[4] Dipartimento di Fisica e Astronomia "Augusto Righi" Viale Berti Pichat 6/2, Bologna, Italy
[5] Université Grenoble Alpes, CNRS, IPAG, F-38000 Grenoble, France
[6] Université Paris-Saclay, Université Paris Cité, CEA, CNRS, AIM, F-91191, Gif-sur-Yvette, France
[7] Universität Heidelberg, Zentrum für Astronomie, Institut für Theoretische Astrophysik, Albert-Ueberle-Straße 2, D-69120 Heidelberg, Germany
[8] Universität Heidelberg, Interdisziplinäres Zentrum für Wissenschaftliches Rechnen, INF 205, D-D-69120 Heidelberg, Germany
[9] INAF-Istituto di Astrofisica e Planetologia Spaziali, Via del Fosso del Cavaliere 100, I-00133, Rome, Italy

Abstract

Low dust opacity spectral indices ($\beta < 1$) measured in the inner envelopes of class 0/I young stellar objects (age $\sim 10^{4-5}$ yr) have been interpreted as the presence of (sub-)millimeter dust grains in these environments. The density conditions and the lifetimes of collapsing envelopes have proven unfavorable for the growth of solids up to millimeter sizes. As an alternative, magnetohydrodynamical simulations suggest that protostellar jets and outflows might lift grains from circumstellar disks and diffuse them in the envelope. We reframe available data for the CALYPSO sample of Class 0/I sources and show tentative evidence for an anticorrelation between the value of $\beta_{1-3\ \mathrm{mm}}$ measured in the inner envelope and the mass-loss rate of their jets and outflows, supporting a connection between the two. We discuss the implications that dust transport from the disk to the inner envelope might have for several aspects of planet formation. Finally, we urge for more accurate measurements of both correlated quantities and the extension of this work to larger samples, necessary to further test the transport scenario.

Unified Astronomy Thesaurus concepts: Interstellar medium (847); Planet formation (1241); Circumstellar dust (236); Stellar jets (1607); Stellar winds (1636); Millimeter astronomy (1061)

1. Introduction

The formation of terrestrial planets and of the rocky cores of giant planets is thought to happen in a core-accretion scenario, a process spanning 10 orders of magnitude in size, where interstellar medium, submicron dust grains grow into kilometer-sized objects. While dust growth has been long thought to take place exclusively in isolated, evolved protoplanetary disks revolving around class II young stellar objects (YSOs), recent observations indicate that dust growth up to millimeter sizes might start in collapsing protostellar envelopes, thus much earlier and further away from host stars than previously thought. Observationally, the slope α of the spectral energy distribution (SED) across (sub-)millimetric wavelengths is a means to interpret interstellar dust properties and its size. Specifically, if (i) dust opacity scales as a power law ($\kappa \propto \nu^\beta$), (ii) the emission is optically thin, and (iii) the Rayleigh–Jeans (RJ) approximation holds, then $\beta = \alpha - 2$ (Natta et al. 2007; Testi et al. 2014). In turn, β depends on dust properties, and strongly on the maximum grain size of the dust population. For the interstellar medium, typically $\beta \sim 1.7$ (Weingartner & Draine 2001). In Class II objects, $\beta < 1$ suggests the presence of millimeter dust grains (e.g., Testi et al. 2014; Macías et al. 2021; Tazzari et al. 2021).

Several authors measured low β values in the inner envelopes (a few 10^2 au) of Class 0/I sources (Kwon et al. 2009;

Miotello et al. 2014; Galametz et al. 2019). Although β also depends on grain composition and porosity, some of the observed values are too low ($\beta < 0.5$) to be explained without considering 100 μm–1 mm grains (e.g., Köhler et al. 2015; Ysard et al. 2019). However, simulations have so far predicted that dust coagulation would be ineffective at the low densities ($n \sim 10^{5-7}$ cm^{-3}) and short timescales (a few 10^5 yr) that characterize these environments (Ormel et al. 2009; Silsbee et al. 2022; Lebreuilly et al. 2023). It will be crucial for the next simulations to test the effects of generally disregarded processes, like the dust back-reaction on the turbulence through gas–dust friction and dust–magnetic-field interaction (Hennebelle & Lebreuilly 2023), to check whether growth remains a viable scenario.

Alternative or concomitant processes must be considered that could contribute to explaining the observed low β. For example, Wong et al. (2016) first presented a simple analytical model to argue that millimeter dust from the disk could be entrained by protostellar outflows and transported to the envelope. Giacalone et al. (2019) also presented an analytical model for the entrainment of dust grains along magnetohydrodynamical (MHD) disk winds, and concluded that grains of ~ 10 μm can be lifted by MHD winds and be transported outward in the disk of T Tauri and Herbig Ae/Be objects. However, their model assumes typical evolved mass outflow rates of $\sim 10^{-8}$ $M_\odot$ yr^{-1}. Since the maximum grain sizes lifted in the envelopes depend linearly on this quantity, it can be much larger in young Class 0/I objects, for which the mass loss rates are orders of magnitude higher. These findings might have found recent confirmation thanks to exquisite JWST

Table 1
Dust Opacity Spectral Indices at 500 au ($\beta_{500\,au}$), Envelope Masses (M_{env}), and Jets and Outflows Mass Loss Rates ($\dot{M}_J$ and $\dot{M}_{OF}$, Respectively) from the Selected Class 0 Sources from the CALYPSO Sample (Maury et al. 2019)

Source	$\dot{M}_J$ (B)[a] $(10^{-7}\,M_\odot\,yr^{-1})$	$\dot{M}_J$ (R)[a] $(10^{-7}\,M_\odot\,yr^{-1})$	$\dot{M}_{OF}$ (B) $(10^{-8}\,M_\odot\,yr^{-1})$	$\dot{M}_{OF}$ (R) $(10^{-8}\,M_\odot\,yr^{-1})$	$\beta_{500\,au}$[b]	M_{env}[b] $(M_\odot)$
L1527	<0.2	<0.2	0.5	0.5	1.41 ± 0.16	1.2
L1157	1.6	2.9	2.5	1.9	1.17 ± 0.18	3.0
SVS13B	<0.1	<0.1	<0.02	<0.02	0.99 ± 0.16	2.8
IRAS2A1	>6.7	<0.1	2.4	1.5	0.82 ± 0.17	7.9
SerpS-MM18a	>11.5	>5.9	12.7	5.1	0.74 ± 0.16	5.4
SerpM-S68Na(1)	>3.3	<0.1	0.12	<0.02	0.66 ± 0.27	11.0
IRAS4B1	1.2	2.3	3.6	1.0	0.62 ± 0.16	4.7
IRAS4A1	⩾4.0	⩾13.7	12.4	11.7	0.54 ± 0.16	12.2
L1448-C	9.7	13.8	7.3	10.1	0.41 ± 0.16	1.9

Notes. The $\dot{M}_{OF}$ are measured in this work and are lower limits as the outflow LV emission is likely optically thick. We report upper limits if no jet/outflow was detected in the CALYPSO data. (1) We do not include SerpM-S68N in the correlation because its SiO (5−4) transition prevents us from identifying high- and low-velocity ranges properly (we note, however, that the correlation is not affected by this point).
[a] From Podio et al. (2021).
[b] From Galametz et al. (2019).

observations of the Tau 042021 edge-on disk, for which Duchene et al. (2023) reported an X-shaped feature in dust scattered whose spatial location is consistent with the Atacama Large Millimeter/submillimeter Array (ALMA) CO line emission tracing an outflow. Their observations suggest the entrainment of $\gtrsim 10\,\mu m$ grains even beyond 300 au. Finally, the findings of these models are supported by Tsukamoto et al. (2021) and Lebreuilly et al. (2023), who arrived at consistent conclusions via three-dimensional MHD simulations. In particular, Tsukamoto et al. (2021) proposed the expression ash fall,[10] referring to the dust grains decoupling from the entrainment outflow and their subsequent fall back in the disk.

Thus, as outflows represent in principle a means to transport submillimeter grains to envelopes, we here explore the unique CALYPSO sample (Maury et al. 2019) to test whether a correlation holds between the observed power of jets and outflows in Class 0 protostars and the dust opacity index in their envelopes.

2. The Sample

The sources that make up our sample are part of the Continuum And Lines in Young ProtoStellar Objects IRAM-PdBI Large Program (CALYPSO[11]; Maury et al. 2019). CALYPSO is a survey of 16 Class 0 sources, located in different star-forming regions ($d \leqslant 450$ pc), observed in three spectral setups (centered at ∼94, 219, and 231 GHz). The observations were carried out with the IRAM Plateau de Bure Interferometer (PdBI). See Maury et al. (2019) for further details. Out of the 16 sources, 9 can be fully characterized for our purposes. Only for these, in fact, a reliable measure of β and of the jets/outflows mass loss rates could be performed ($\dot{M}_J$, $\dot{M}_{OF}$) (Table 1). Among the sources considered in this study, seven are in binary or multiple systems. We report considerations on their multiplicity in Appendix A.

While this is a low number of statistics, we note that CALYPSO is unique in its uniformity and is the only survey for which the SiO (5–4) transition is systematically targeted to detect the high-velocity jets of a sample of protostars (see

Section 4). This allows us to perform the jets/outflows analysis as explained in Section 4 and have deep enough continuum data sets with which Galametz et al. (2019) measured dust optical properties. Finally, we note that the CALYPSO data for the sources we consider here have been self-calibrated as explained in Section 2 of Maury et al. (2019), and the self-calibrated data has been later used in Galametz et al. (2019) and Podio et al. (2021), i.e., the works that have measured the dust opacity spectral index β and the jets' mass loss rates $\dot{M}_J$ that we also consider in this work.

3. The Dust Opacity Spectral Index

As stated in Section 1, the dust opacity spectral index β can be derived starting from the radio spectrum of a source and carries dependencies on the properties of interstellar dust, such as the maximum grain size of the distribution. Galametz et al. (2019) used CALYPSO 1.3 and 3.2 millimeter continuum observations to constrain β and infer the maximum dust grain sizes in the protostellar envelopes of the sources we consider in this work, up to ∼2000 au radial distances from the central protostars. While we report on the details of their measurements in Appendix B for completeness, we here briefly summarize them for the reader's convenience.

They measured β including a temperature correction that accounts for discrepancies from the Rayleigh–Jeans approximation due to low envelope temperatures:

$$\beta = \frac{\log_{10}[(F_{\nu_2}/B_{\nu_2}(T))/(F_{\nu_1}/B_{\nu_1}(T))]}{\log_{10}\nu_2 - \log_{10}\nu_1}, \quad (1)$$

where $\nu_2 = 231$ GHz and $\nu_1 = 94$ GHz are the representative frequencies of the PdBI observations, F_ν is the flux at each frequency. The term $B_\nu(T)$ is the value of the Planck function at a temperature T that depends on the radial distance from the central protostar[12] ($T \propto r^{-0.4}$), evaluated at frequency ν_i. For each envelope, they measured β across scales and reported best-fit linear models to extrapolate β at any other scale. We report the final estimated envelope-only β values at 500 au in

---

[10] Continuing Tsukamoto et al. (2021) nomenclature, we thus propose outflows as "chimney flues" in the title of this work.
[11] https://irfu.cea.fr/Projets/Calypso/Welcome.html

---

[12] In brief, Galametz et al. (2019) assumed this temperature profile based on the radiative transfer postprocessing of dusty envelopes from Motte & André (2001).

Table 1. We note that β also depends on the extent of porosity and on the composition of both grain bulk and ice mantles (e.g., Natta et al. 2007). However, the lowest values observed by Galametz et al. (2019) are only reconcilable with laboratory experiments in which the sizes of the dust grains are $\gtrsim 100\ \mu$m, regardless of ice mantle properties (Köhler et al. 2015; Ysard et al. 2019). The effect of porosity would also not affect the interpretation of low β as being due to large grain sizes (e.g., Birnstiel et al. 2018).

4. Jets and Outflows Mass Loss Rates

In this section, we report previous measurements of jets energetics for the CALYPSO sample and present new ones for their low-velocity outflow counterparts. We note that we are interested in the instantaneous mass loss rates of these components rather than their total ejected mass, hence we do not complement the CALYPSO observations with single dish data. This is the case because we aim to investigate a link between the presently observed low β values of Galametz et al. (2019) and the continuous flow of material along jets and outflows. The mass loss rates are constant along the jets/outflows extension since mass needs to be conserved, and we measure the latter (outflow) as Podio et al. (2021) measured the former (jet), i.e., at the first peak of the respective tracer emission, to minimize the contribution of possible gas entrained along the jet. The positions of these peaks are in Table 4 of Podio et al. (2021). For the reader's convenience, we note that the maximum recoverable scale of the observations is reported to be about $8\overset{''}{.}0$ (Podio et al. 2021). Based on the SiO (5–4) transition at the innermost knots of the blue- and red-shifted lobes, Podio et al. (2021) defined the high-velocity (HV) ranges, where the emission probes the jet, for all sources associated with SiO (see their Figure C.1 and Table 4). In this work, we define the outflow as the emission on the complementary low-velocity (LV) ranges. In Figure 1, we show the spatial distribution of CO (2–1) toward L1448-C, obtained integrating on the LV and HV ranges: HV CO traces the collimated jet, which is believed to originate from the inner disk region, while LV CO probes the wide-angle outflow, which is likely to arise from a more extended disk region. The HV ranges for all the CALYPSO sources are listed in Table 4 of Podio et al. (2021).

At this point, Podio et al. (2021) estimated the $\dot{M}_{\rm J}$, in the blue (B) and red (R) lobes. Here, we apply the same methodology to infer the LV outflows $\dot{M}_{\rm OF}$ of the sources in the CALYPSO sample, for the first time. The beam-averaged CO column densities in the jet and outflow, $N_{\rm CO}$, are derived from the integrated line intensities on HV and LV, respectively. We assume local thermodynamic equilibrium (LTE) at a fixed excitation temperature, $T_{\rm K} = 100$ K for HV jets (e.g., Cabrit et al. 2007), and $T_{\rm K} = 20$ K for LV outflows (e.g., Bachiller et al. 2001), and that the emission is optically thin. The jet and outflow mass loss rates are computed as (Lee et al. 2007; Podio et al. 2015):

$$\dot{M} = 1/\sqrt{C} \cdot m_{\rm H_2} \cdot (N_{\rm CO}/X_{\rm CO}) \cdot b_t \cdot V_{\rm tan}, \qquad (2)$$

where $1/\sqrt{C}$ accounts for compression in the shocks ($C = 3$), $m_{\rm H_2}$ is the mass of molecular hydrogen, $X_{\rm CO} = 10^{-4}$ the assumed CO abundance with respect to H_2, b_t the beam size perpendicular to the jet, and $V_{\rm tan}$ the tangential jet/outflow velocity. The latter is obtained by correcting for inclination the jet/outflow velocities, assumed to be 100 km s^{-1} for the HV jet, and 10 km s^{-1} for the LV outflow. The inclination is derived from the ratio between the assumed jet velocity and its radial component from the HV spectra (see Table 4 of Podio et al. 2021).

For the HV jets, Podio et al. (2021) identified the sources for which $\dot{M}_{\rm J}$ is a lower limit by comparing CO and SiO spectra. The estimated rates carry a factor of 3–10 of uncertainty due to the calibration of the parameters of Equation (2). The LV outflow emission is likely optically thick; therefore, the estimated $\dot{M}_{\rm OF}$ must be considered as lower limits. We can estimate the uncertainty introduced by optical depth using ^{13}CO emission in the assumption that it is optically thin. For two sources only (IRAS4A1 and IRAS4B1), ^{13}CO is detected along the jet (see the maps in Maret et al. 2020). For these two sources, we can reliably estimate the ^{12}CO/^{13}CO ratio, hence opacity. We find $\tau_{\rm IRAS4A1}^{(R)} = 6$, $\tau_{\rm IRAS4A1}^{(B)} = 18$, $\tau_{\rm IRAS4B1}^{(R)} = 15$, $\tau_{\rm IRAS4B1}^{(B)} = 7$. These values imply $\dot{M}_{\rm OF}$ higher by a factor at least $\sim$6–18. Since we cannot repeat this analysis for all sources, we here stress that the derived $\dot{M}_{\rm OF}$ (in Table 1 and Figure 2) are lower limits and we consider the jets to be a more robust proxy of the effective mass loss rates of each protostar. Observations of optically thin tracers of the low-velocity outflows will be key to further test the correlation we propose.

5. A Tentative Anticorrelation

Modern theoretical efforts have shown how growing dust grains in protostellar envelopes is problematic due to the lifetimes and densities of these environments (Ormel et al. 2009; Bate 2022; Silsbee et al. 2022; Lebreuilly et al. 2023). If millimeter dust, implied by recent measurements of low dust opacity spectral indices in envelopes (Miotello et al. 2014; Galametz et al. 2019), cannot grow at envelope scales, alternative processes might explain their presence therein. We here show a tentative anticorrelation between β with $\dot{M}_{\rm J}$ and $\dot{M}_{\rm OF}$, potentially supporting a scenario in which protostars launching powerful outflows can lift millimeter grains into their envelopes. Figure 2 shows the β indices found by Galametz et al. (2019) as a function of $\dot{M}_{\rm J}$ and $\dot{M}_{\rm OF}$ summed over the blue and red lobes (see Section 2). The values are reported in Table 1. We do not include SerpM-S68N because SiO (5–4) emission in Podio et al. (2021) is only at low velocities, likely due to the system inclination, thus impeding the identification of the LV and HV.

The resulting Pearson correlation coefficients are:

1. $\rho_J = -0.73 \pm 0.27$ ($\beta_{500\,{\rm au}}$, $\dot{M}_{\rm J}^{R+B}$)
2. $\rho_{\rm OF} = -0.68 \pm 0.28$ ($\beta_{500\,{\rm au}}$, $\dot{M}_{\rm OF}^{R+B}$).

We evaluate the statistical significance of such a correlation by means of a two-tailed Student's t-test, where the null hypothesis is that $\rho = 0$ (against $\rho \neq 0$). We reject the null hypothesis at $p < 0.04$ level in the jet case, and at the $p < 0.06$ level for the outflows. These tentative correlations might support a dust transport scenario from young disks to their embedding envelopes.

Alternative explanations to the observed tentative correlation are possible in case these two share correlations with other quantities. Bontemps et al. (1996) found a correlation between the envelope mass of Class 0/I YSOs and the CO momentum flux of their outflows. Since Galametz et al. (2019) observed a correlation between β and envelope mass of CALYPSO
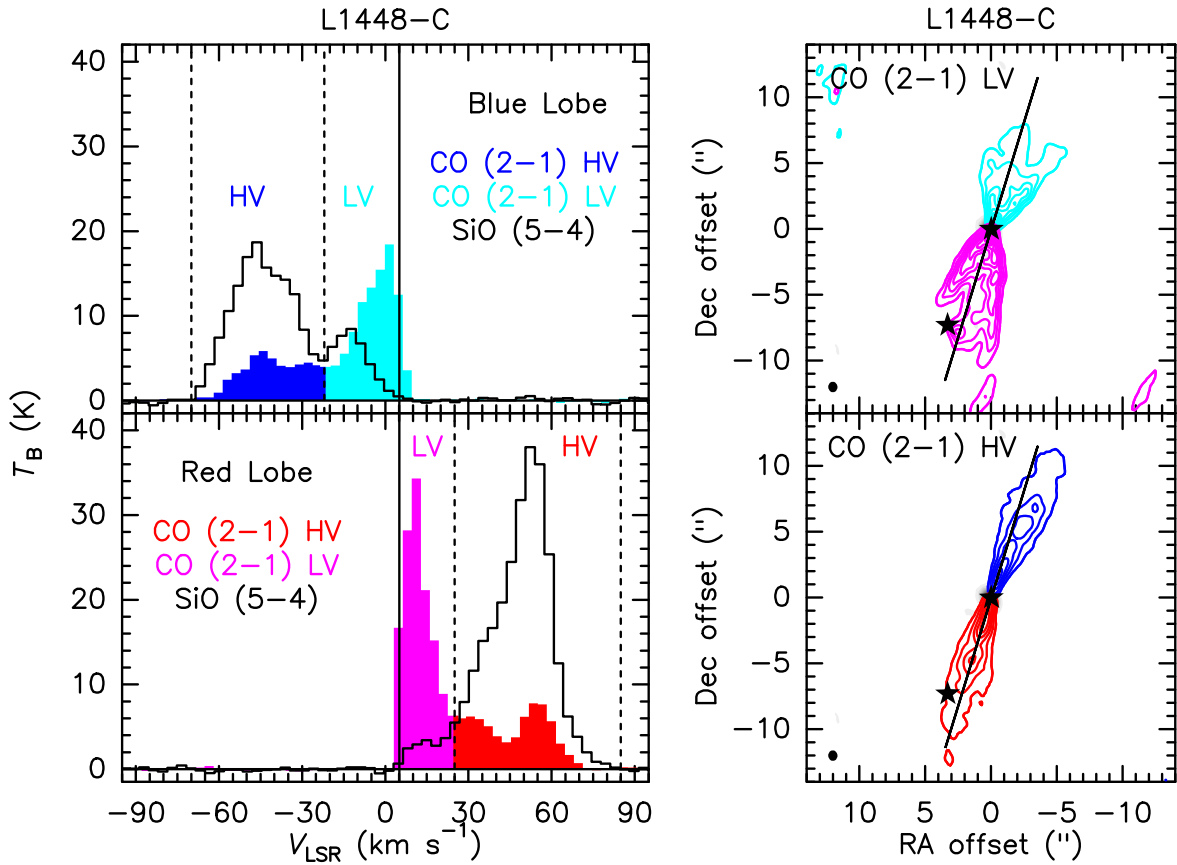
Figure 1. The L1448-C jet and the outflow, as imaged with PdBI in CO $(2-1)$ and SiO $(5-4)$. Left panels: CO (blue, cyan, magenta, and red) and SiO (black) spectra at the position of the blue-shifted and red-shifted SiO knots located closest to the driving source (from Podio et al. 2021). The horizontal and vertical solid lines indicate the baseline and systemic velocity, $V_{sys} = +5.1$ km s^{-1}, respectively. The vertical black dotted lines indicate the high-velocity (HV, blue/red) and low-velocity (LV, cyan/magenta) ranges, which trace the jet and the outflow, respectively. The definition of LV and HV ranges is based on the SiO $(5-4)$ emission (see the main text). Right panels: maps of CO $(2-1)$, integrated on the LV (top panel) and HV (bottom panel) ranges. First contours and steps are 5σ, corresponding to 1 Jy km s^{-1} beam^{-1}. The black stars indicate the positions of the protostars L1448-C (at the center) and L1448-CS. The black solid line shows the jet/outflow PA (Podio et al. 2021). The beam size is in the bottom-left corner.

sources, then the tentative correlation we show in Figure 2 might be the combined result of these underlying relationships. However, it remains unclear whether the fundamental causal correlation is the one between the dust opacity spectral index and envelope mass or the mass loss rates, as presented here. Moreover, the $\beta - \dot{M}_{OF}$ correlation in Figure 2 might be caused by an underlying $\dot{M}_J - \dot{M}_{OF}$ correlation. Such a correlation cannot be quantified here, given that the estimated $\dot{M}_{OF}$ are lower limits. To rule out possible contamination of the correlation from any dependence of the measured β and mass loss rates on the inclination of the source (disk/jet), we reject possible underlying correlations in Appendix D.

6. Discussion

We here further discuss our findings and the conditions that need to be met in order for the proposed dust transport to happen.

6.1. When and Where Do Transported Grains Grow?

If outflows are lifting millimeter (or larger) dust grains into the envelopes of Class 0 objects, these must have first grown in the disk. Brauer et al. (2008) studied dust coagulation in the first 1 Myr of disk evolution at representative 1, 10, and 100 au scales and found that millimeter dust grains dominate the dust size distribution already after few 10^3 yr in the inner 1 au of the

disk. Lebreuilly et al. (2023) considered several dust size distributions and simulated their early evolution during protostellar collapse under the effects of turbulent, Brownian, and radial motions. They found that millimeter grains are formed at $\lesssim 0.1$ au scales in the few years after the first Larson core formation starts. Laboratory experiments have been performed to constrain the stickiness of dust grains in the disk inner regions. When heated at 1000 K, dust grains become super dry and their stickiness can increase up to a factor of 100, thus providing the conditions to grow even larger agglomerates (Bogdan et al. 2020; Pillich et al. 2021). These temperatures are typically reached in the inner ~ 0.1 au of low-mass protostellar disks. At these distances, both jets and outflows could lift grains. Indeed, the typical footpoint of a jet is much closer to the star than are the outflows. For example, Lee et al. (2017) measured a 0.05–0.3 au footpoint radius for the high-velocity SiO jet in the Class 0 HH212 source. Low-velocity outflows, instead, likely extend to a wider disk region out to radii of even 20–40 au (Bjerkeli et al. 2016; Tabone et al. 2017; Lee et al. 2018), and thus could entrain grains from a larger reservoir.

6.2. Can Outflows Lift Millimeter Grains?

Wong et al. (2016) and Giacalone et al. (2019) presented an analytical treatment in which they explored the conditions for the uplifting of dust grains along outflows. Wong et al. (2016)
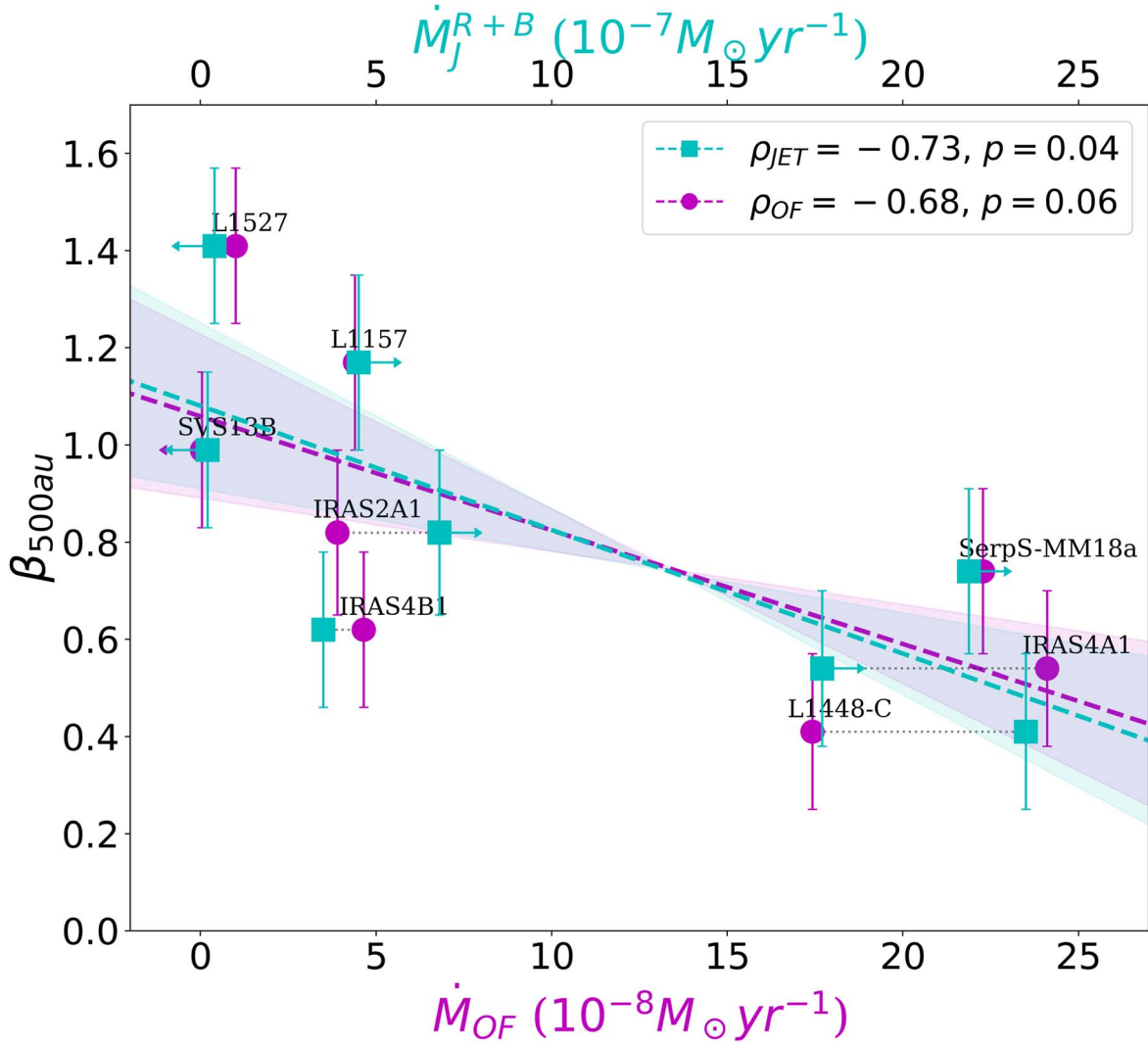
Figure 2. The total (red plus blue lobe) jet mass loss rates (cyan points, upper x-axis) and outflows mass loss rates (magenta points, lower x-axis) around young Class 0 sources anticorrelates with β (y-axis) of their inner envelopes ($\beta_{500\,au}$). For each source, a dotted gray line connects the corresponding jet and outflow rates. Source names are on top of the corresponding magenta point. The best-fit linear relations are shown in cyan and magenta, for outflows and jets, respectively.

presented the critical mass of the protostar for which, if $M_* < M_{cr}$, grains of a given size could be entrained against gravity (see their Equation 7). Another analytical model, by Giacalone et al. (2019), reported an equation to compute the maximum grain size a_{max} that a given wind can uplift against the gravity of a star of mass M_*. We report the latter for the reader's convenience:

$$a_{max} \approx 0.35\,\mu m \left(\frac{M_*}{M_\odot}\right)^{-1} \left(\frac{\dot{M}}{10^{-8}M_\odot\ yr^{-1}}\right) \left(\frac{T_{gas}}{200\ K}\right)^{0.5}$$
$$\times \left(\frac{r}{au}\right)^{-0.25} \left(\frac{(z/r)}{0.06}\right)^{-1} \left(\frac{\log(r_+/r_-)}{10^3}\right)^{-1}, \quad (3)$$

where $\dot{M}_\odot/yr$ is the mass loss rate of the outflow, T_{gas} is the gas temperature, r is the launching footpoint, z/r the disk flaring ratio, r_+/r_- the ratio between disk's outer and inner edge. See Giacalone et al. (2019) for the details. We notice that the three sources of our sample with the largest outflow mass loss rates ($\gtrsim 2 \times 10^{-7} M_\odot\ yr^{-1}$) have $\beta < 0.8$. If we consider this value in Equation 3, and we fix $M_* = 1\ M_\odot$, $T_{gas} = 20\ K$ at the outflow's base, $r = 1$ au, $z/r = 0.1$, $r_+ = 50$ au (typical

Class 0 disk radius, e.g., Maury et al. 2022), and $r_- = 0.1$ au, we obtain $a_{max} \gtrsim 150\,\mu m$. Since outflow mass loss rates are lower limits due to optical depth effects, a_{max} could be higher by even an order of magnitude. We refrain from evaluating Equation (3) source by source since it was derived for class II objects rather than class 0/I, and because most parameters suffer from large uncertainties for young sources. Thus, at face value, assuming standard parameters, grains larger than $100\,\mu m$ could be lifted for the sources with the highest mass loss rates (and lowest betas).

Similar findings for the maximum sizes of dust grains entrainable by outflows were reported by Lebreuilly et al. (2020) and Tsukamoto et al. (2021). They both performed MHD simulations. Lebreuilly et al. (2020) ran their setup including large grains to account for growth that might have happened at earlier times, while Tsukamoto et al. (2021) modeled dust coagulation. They both found that large grains in the inner region of the disk (a few $100\,\mu m$ to 1 cm) can be entrained. These grains then decouple from the gas and are ejected from the outflow into the envelope, before falling back into the disk-like ash fall, as coined by Tsukamoto et al. (2021).

6.3. Do Grains Survive the Transport?

Given their lower velocities and temperatures, as well as a wider entraining base, outflows seem to be the preferred mechanism to lift dust grains from protoplanetary disks to the inner envelopes of young protostars (Wong et al. 2016; Lebreuilly et al. 2020; Tsukamoto et al. 2021). The tentative β–$\dot{M}_{OF}$ correlation we present in Figure 2 might support this scenario. The observed β–$\dot{M}_J$ correlation might either mean that jets are contributing to the mechanism or that they share an underlying correlation with the outflows. We thus discuss here if lifted dust grains would survive the transport along jets. Given the much lower speeds and temperatures of outflows, their survival to transport along the latter is a consequence.

The destruction of silicon-bearing dust grains in shocks has been identified as the mechanism that enriches SiO in the interstellar medium and makes of this molecule a key jet tracer (e.g., Flower & Forêts 1994; Caselli et al. 1997; Schilke et al. 1997). However, shock models predict that only a small fraction ($<10\%$) of grains is destroyed in the mild shocks along jets, with typical velocities of $20-50$ km s^{-1} and preshock gas densities of 10^4–10^6 cm^{-3} (e.g., Gusdorf et al. 2008a, 2008b; Guillet et al. 2011).

In the wide grid of models explored by Gusdorf et al. (2008a), where the shock velocities range 20 km s^{-1} $<v_s< 50$ km s^{-1} and the preshock gas densities are in the interval 10^4 cm^{-3} $< n_H < 10^6$ cm^{-3}, no more than 5% of Si is released in the gas phase by sputtering. Taking into account shattering and vaporization of the grains in grain–grain collisions may enhance the fraction of grains destroyed to $\sim 8\%$ (Guillet et al. 2011). These shock models reproduce the typical SiO abundances estimated in protostellar shocks that span from a few 10^{-8} and a few 10^{-7} (e.g., Bachiller & Pérez Gutiérrez 1997; Gibb et al. 2004; Tafalla et al. 2010). Recent high angular resolution observations, e.g., in CALYPSO, indicate that SiO may reach abundances $>5 \times 10^{-6}$ in jets, which requires either dust-free jets or the fraction of grains sputtered in shocks being larger than 10% (for [Si/H]$_\odot \sim 3.5 \times 10^{-5}$; Holweger 2001).

Finally, Wong et al. (2016) studied whether (sub-)millimeter dust seeds would survive grain–grain collisions in the envelope, after reaching the transport limit velocity ($v \sim 0.5$ km s^{-1}), given by the gravity-drag equilibrium along the outflow. Making use of the shattering model of Kobayashi & Tanaka (2010), they concluded that millimeter-sized dust grains could survive in the envelope environment: only a fraction as small as 10% might be destroyed.

Thus, it seems reasonable that a large percentage of dust grains could survive the transport along outflows and even jets, being only partially eroded by collisions with both other grains and gas molecules in the latter. However, we note that there is a strong necessity for dust laboratory and modeling studies to assess the effects of high temperatures in the inner disk if submillimeter dust were lifted from inner outflow footpoints. In particular, it will be crucial to test whether the high temperatures would sublimate grain's mantles materials causing them to further shrink in size.

6.4. Potential Implications

The possibility that protostellar outflows lift large millimeter grains from the disk into the envelopes of YSOs can have several implications for the evolution of dust throughout the system. The outwards transport of dust can extend the timescales of grain growth in disks, limited by the meter barrier problem; it can affect the physical properties of grains as they are transported upward away from the optically thick disk; and it can contribute to explaining the mixing of the mineralogy of outer disks, like the one found in meteorites in the solar system.

First, the orbital dynamics of dust grains orbiting in a disk depends on their Stokes number, defined by their composition, density, and size. When particles grow in size, they experience a larger and larger headwind that slows them down and causes an inward orbit shift, known as radial drift. In a typical disk orbiting a 1 $M_\odot$ star, radial drift velocities of solids at 1 au reach a maximum for meter-sized boulders, thus causing intermediate solids to rapidly fall toward the central star in timescales much faster than the ones estimated for planet cores formation (Weidenschilling 1977). At larger radii, this peak velocity is reached for even smaller pebbles. If outflows were uplifting grains in a continuous recycle of dust to the outer disk, this would set back grown millimeter grains in its outskirts and contribute to stretching the available time span to form larger agglomerates, as already proposed by Tsukamoto et al. (2021). Moreover, if young protoplanetary disks harbor ring substructures that act like dust traps (as is the case for, e.g., GY91 from Sheehan & Eisner 2018 or IRS63 from Segura-Cox et al. 2020), then outward-transported grains will be halted on their drift back toward the inner disk at one of these substructures, potential birthplaces of planetesimals via streaming instabilities (Carrera et al. 2021; Chambers 2021).

Second, transported dust grains would undergo physical and chemical reprocessing once in the envelope. While they are partially shielded from the radiation of the star in the dense disk, they are going to be lifted in the much thinner envelope and the different energy and intensity of stellar radiation impinging onto them could change their structural and compositional properties. Furthermore, the grains would be transported from the warm inner disk to the colder envelopes where molecular freeze-out could form ice mantles.

Last, the uplifting and outward transport of inner disk grains represents a potential explanation for the discovery of crystalline grains in the outskirts of protoplanetary disks, where the temperatures are too low to explain spectral observations of silicate lines (e.g., Apai et al. 2005; Sargent et al. 2009). Along the same line, Trinquier et al. (2009) and Williams et al. (2020) observed anomalous abundances of ^{46}Ti, ^{50}Ti, and ^{54}Cr isotopes in outer solar system chondrules (millimeter-sized meteorite inclusions). Since calcium–aluminum inclusions, which formed in the inner solar system, consistently show high abundances in both isotopes, they proposed a mixing of solar nebula material in the early stages of formation. In the same direction are the recent findings of Hellmann et al. (2023), who show that carbonaceous chondrites display correlation in different isotopes abundances, which can be explained by mixing of refractory inclusions, chondrules, and chondrite-like matrix. They thus highlight the need for a mechanism to transport these constituents from the inner disk to its outskirts and trap them in rings where the meteorites would form. If dynamical barriers to outward viscous transport were present, such as the core of a Jupiter-like planet, protostellar outflows might have played this transport role: the grains extracted by outflows from inner disk regions will later fall back onto the disk out to larger radii.

7. Conclusions

Recently, extremely low dust opacity indices have been observed at few hundred au scales in the envelopes of Class 0 sources, and have been interpreted as the presence of millimetric dust grains (Galametz et al. 2019). Since theoretical models seem to discard the possibility of growing millimeter grains at the densities typical of protostellar envelopes (e.g., Ormel et al. 2009; Silsbee et al. 2022), we propose here a possible observational test to an alternative explanation, the transport of dust from the disk into envelopes via protostellar outflows. The mechanism has been studied analytically by Wong et al. (2016) and Giacalone et al. (2019) and is supported by numerical simulations of Lebreuilly et al. (2020) and Tsukamoto et al. (2021).

We show a tentative anticorrelation between protostellar envelopes β and their mass loss rates driven by jets and outflows. Such a correlation can be interpreted as supporting a scenario in which protostellar outflows transport large disk grains into the envelopes of young sources.

If protostellar outflows are indeed lifting millimeter grains in the envelopes of young sources, implications are important for the meter-size barrier problem, the reprocessing of dust during its life cycle, and for material mixing throughout planetary systems, as already suggested for the solar system (see Section 6). While further measurements of both dust opacity index and mass loss rates will be key in either confirming or disproving such a correlation, we here stress how we explored this possibility with a unique sample in this regard, for which uniform observations, reduction, and analyses were carried out. ALMA and JWST synergies will be key to better constrain both dust properties and jets/outflows energetics in a larger sample of young sources.

Appendix A
Binary Protostars

When stars form from the collapse of gas clouds, fragmentation of dense cores often leads to binary or multiple systems. It is estimated that the fraction of stars with at least one companion in the galaxy is between $\sim$20% for M-type sources up to $\sim$90% for O-type sources (Offner et al. 2023). The protostars of the CALYPSO sample are no exception. The PdBI observations beam allowed Maury et al. (2019) to separate systems in the maps with separations larger than $\sim$60 au in Taurus, $\sim$90 au in Perseus, and 132 au in Serpens South. For Serpens Main, the systems (SerpM-SMM4, SerpM-S68N) are probed down to distances smaller than 160 au. These spatial resolutions are based on distance measurements from Zucker et al. (2019) for Taurus (140 pc), Ortiz-León et al. (2018a) for Perseus (290 pc), Ortiz-León et al. (2023) for Serpens South (441 pc) and Ortiz-León et al. (2018b) for Serpens Main (436 pc). Moreover, on the large-scale end, they were sensitive to companions up to $\sim$1500–2800 au, depending on the region. They finally classified IRAM04191, L1521F, L1527, L1157, GF9-2, and SerpS-MM22 as single sources. On the contrary, L1448-2A, L1448-N, L1448-C, IRAS4A, IRAS4B, SerpS-MM18, SVS13B, and IRAS2A were classified as having a companion. For each protostar considered in this work, we report the distance of their companion (s), if any, in Table 2. We note that the tightest binary systems have not been considered here since either a measurement of β, $\dot{M}_J$, or $\dot{M}_{OF}$ was impractical in the studies of Galametz et al. (2019), Podio et al. (2021), or our own, respectively. While most sources of this study are well-resolved binaries, their separation is usually closer than the extent of their envelopes, thus they share a common envelope. The only exceptions are SVS13B and IRAS4B1, for which the companion(s) have much wider separations. For all the sources considered in this work, and that enter the tentative correlation described in Section 5, the source of jets and outflows was well resolved (e.g., see Figure 1) and the measurement of β could be performed after model subtraction of the secondaries. Furthermore, we note that the low β of Galametz et al. (2019) are measured in the inner envelope of each protostar and thus far from possible contamination of the much larger common envelope (see Section 3).

Table 2
Stellar Companions Associated to the Protostars Considered in This Work

Source	Companion(s) Name: Distance
L1527	…
L1157	…
SVS13B	SVS13A: 3500 au, SVS13C: 4500 au
IRAS2A1	IRAS2-A2: 143 au
SerpS-MM18a	SerpS-MM18b: 2600 au[a]
SerpM-S68Na	SerpM-S68Nb: 5000 au, SerpM-S68Nc: 8300 au
IRAS4B1	IRAS4-B2: 3500 au
IRAS4A1	IRAS4-A2: 420 au
L1448-C	L1448-C(S): 2000 au

Notes. The separations are reported in Maury et al. (2019).
[a] Note that the physical separation of the SerpS-MM18 reported therein should instead be 4420 au, given the most up-to-date distance measurements of the Serpens South region Ortiz-León et al. (2023).

Appendix B
Details on β Measurements of Galametz et al. (2019)

Galametz et al. (2019) measured the dust opacity spectral index in a sample of Class 0/I protostellar envelopes. First, for β to be a trustworthy proxy of the maximum grain size of a dust distribution, the emission over which the radio spectrum is sampled needs to be optically thin. Hence, they estimated the envelopes' optical depths and found τ well below 0.1 at scales of a few hundred astronomical units for every source (see their Figure 2). To make sure the measured β would be representative of the envelope alone, Galametz et al. (2019) subtracted both the emission of binary companions (see Appendix A) and circumstellar disks. The companions were subtracted by fitting and removing a Gaussian model centered on the secondary sources from the visibilities (further details in Maury et al. 2019). Second, the contribution of the circumstellar disk orbiting the target protostar was evaluated in the uv

space as the mean of the amplitudes after 200 kλ and subtracted from the shorter baseline visibilities. They test and comment on the robustness of such a correction in their Section 4, where they assess that considering the mean of the amplitudes in slightly different ranges of the long-baseline end of the visibilities would not affect their results. Moreover, they subtracted the non-thermal dust contribution by extrapolating literature centimeter data for each source, as shown in their Table A.1.

Appendix C
Jets High-velocity Ranges

In Table 3, we report the velocity ranges in which we identify high- and low-velocity SiO line emission. These ranges were then used to derive mass loss rates from the CO line emission.

Table 3
Table of Identified High-velocity Ranges from the SiO Jet Emission for Each Source (from Table 4 in Podio et al. 2021)

Source	Lobe	HV Range (km s^{-1})	$V_{\rm sys}$ (km s^{-1})
L1527	B	−21.8/−11.8 7	+5.7
	R	+17/+27	
L1157	B	−60/−20	+2.6
	R	+30/+70	
SVS13B	B	−37/+8.5	+8.5
	R	+8.5/+58	
IRAS2A1	B	−32/−9	+7.5
	R	…	
SerpS-MM18a	B	−17/−2	+8.1
	R	+21/+32	
SerpM-S68N	B	−7/+5	+9.2
	R	+12/+21	
IRAS4B1	B	−30/−5	+6.8
	R	+16/+50	
IRAS4A1	B	−30/−10	+6.3
	R	+30/+70	
L1448-C	B	−70/−22	+5.1
	R	+25/+85	

Note. Based on these ranges, the high- and low-velocity emission of the CO is defined in order to derive the mass loss rates. Only the blue lobe is detected for IRAS2A1. For L1527, no SiO is detected. Therefore the LV range is defined based on the CO emission, while the HV range is assumed to extend $+/-10$ km s^{-1} with respect to the largest velocity detect in the LV.

Appendix D
Inclination Dependencies

As a reality check for our correlations, we tested whether any underlying correlation exists between the reported (β, $\dot{M}_J$) or measured quantities ($\dot{M}_{OF}$) and the inclination of the sources of our sample. To derive the mass loss rates of outflows and jets, in fact, this work and Podio et al. (2021) assumed velocities of 10–100 km s^{-1}, respectively (see Section 4). Such an approach ensures a uniform method to derive the rates, rather than making assumptions on the inclinations of the jets and outflows since current estimates are either unavailable or very uncertain. Thus, in this section, we check for potential correlation between the quantities involved in our proposed correlation. The inclinations we use have been collected from a number of works. Where more than one estimate was available based on different methods, we reported an average value. If no uncertainty was reported in the literature, for example, because the estimate is only of qualitative nature (e.g., for IRAS2A1 reported by Codella et al. 2014), we plot no error bar.

Inclinations for IRAS4A and IRAS4B were reported by Yıldız et al. (2012) and Marvel et al. (2008). The inclination for the jet of SVS13B was reported to be ~71° by Segura-Cox et al. (2016), while Podio et al. (2016) measured the one for L1157 at ~73°. Yoshida et al. (2021) constrained the inclination of L1448-C to be ~34 and ~46 for the blue- and red-shifted lobes, respectively (in this case, we report the main value and scatter between the two). The inclination of L1527 is well constrained to be almost perpendicular to the sky plane (e.g., 85° in Ohashi et al. 1997). Finally, Plunkett et al. (2015) and Podio et al. (2021) independently and qualitatively assessed that the jet of SerpM-SMM18a lays in the plane of the sky, so we set it $i = 90°$. Figure 3 summarizes the relationship between the inclinations and $\dot{M}_J$, $\dot{M}_{OF}$, or β for the CALYPSO sample. While a hint for a correlation is seen for the (β, inclination) pair, only a combination of underlying correlations for both β and mass loss rates with inclination would justify the correlation between β and mass loss rates. We thus conclude that possible inclination biases are not driving the correlation in Figure 2.
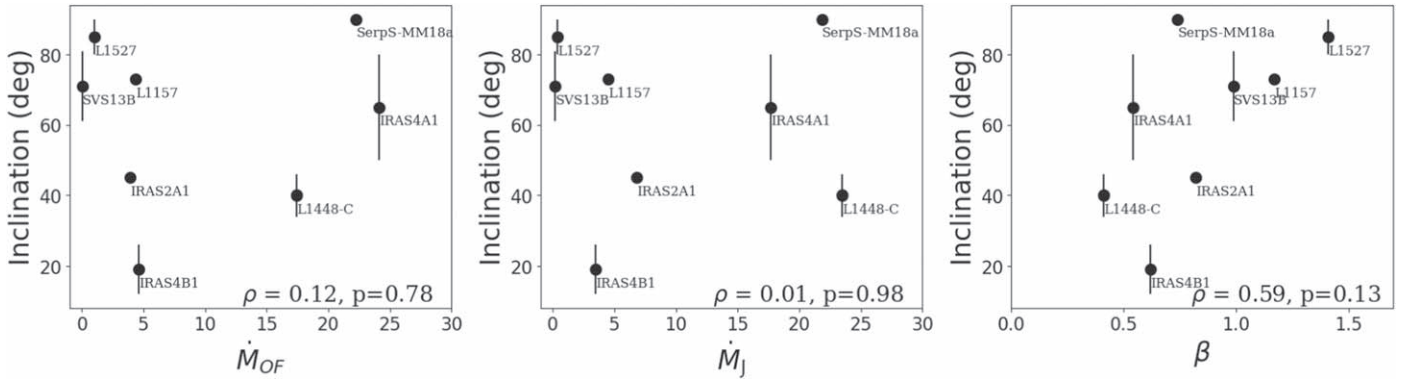

Figure 3. Scatter plot of the jets mass loss rates for the CALYPSO sample with inclinations of their jets (left), and same for the outflows mass loss rates (center) and dust opacity spectral index (right). The Pearson correlation coefficient and related p-value are reported in the lower right of each panel.

ORCID iDs

L. Cacciapuoti ⓘ https://orcid.org/0000-0001-8266-0894
L. Podio ⓘ https://orcid.org/0000-0003-2733-5372
C. Codella ⓘ https://orcid.org/0000-0003-1514-3074
A. J. Maury ⓘ https://orcid.org/0000-0002-3801-8754
M. De Simone ⓘ https://orcid.org/0000-0001-5659-0140
P. Hennebelle ⓘ https://orcid.org/0000-0002-0472-7202
U. Lebreuilly ⓘ https://orcid.org/0000-0001-8060-1890
R. S. Klessen ⓘ https://orcid.org/0000-0002-0560-3172
S. Molinari ⓘ https://orcid.org/0000-0002-9826-7525

References

Apai, D., Pascucci, I., Bouwman, J., et al. 2005, Sci, 310, 834
Bachiller, R., & Pérez Gutiérrez, M. 1997, ApJL, 487, L93
Bachiller, R., Pérez Gutiérrez, M., Kumar, M. S. N., & Tafalla, M. 2001, A&A, 372, 899
Bate, M. R. 2022, MNRAS, 514, 2145
Birnstiel, T., Dullemond, C. P., Zhu, Z., et al. 2018, ApJL, 869, L45
Bjerkeli, P., Jørgensen, J. K., & Brinch, C. 2016, A&A, 587, A145
Bogdan, T., Pillich, C., Landers, J., Wende, H., & Wurm, G. 2020, A&A, 638, A151
Bontemps, S., Andre, P., Terebey, S., & Cabrit, S. 1996, A&A, 311, 858
Brauer, F., Dullemond, C. P., & Henning, T. 2008, A&A, 480, 859
Cabrit, S., Codella, C., Gueth, F., et al. 2007, A&A, 468, L29
Carrera, D., Simon, J. B., Li, R., Kretke, K. A., & Klahr, H. 2021, AJ, 161, 96
Caselli, P., Hartquist, T. W., & Havnes, O. 1997, A&A, 322, 296
Chambers, J. 2021, ApJ, 914, 102
Codella, C., Maury, A. J., Gueth, F., et al. 2014, A&A, 563, L3
Duchene, G., Menard, F., Stapelfeldt, K., et al. 2023, arXiv:2309.07040
Flower, D. R., & Forêts, G. P. D. 1994, MNRAS, 268, 724
Galametz, M., Maury, A. J., Valdivia, V., et al. 2019, A&A, 632, A5
Giacalone, S., Teitler, S., Königl, A., Krijt, S., & Ciesla, F. J. 2019, ApJ, 882, 33
Gibb, A. G., Richer, J. S., Chandler, C. J., & Davis, C. J. 2004, ApJ, 603, 198
Guillet, V., Pineau Des Forêts, G., & Jones, A. P. 2011, A&A, 527, A123
Gusdorf, A., Cabrit, S., Flower, D. R., & Pineau Des Forêts, G. 2008a, A&A, 482, 809
Gusdorf, A., Pineau Des Forêts, G., Cabrit, S., & Flower, D. R. 2008b, A&A, 490, 695
Hellmann, J. L., Schneider, J. M., Wölfer, E., et al. 2023, ApJL, 946, L34
Hennebelle, P., & Lebreuilly, U. 2023, A&A, 674, A149
Holweger, H. 2001, in AIP Conf. Ser. 598, Joint SOHO/ACE workshop "Solar and Galactic Composition", ed. R. F. Wimmer-Schweingruber (Melville, NY: AIP), 23
Kobayashi, H., & Tanaka, H. 2010, Icar, 206, 735
Köhler, M., Ysard, N., & Jones, A. P. 2015, A&A, 579, A15
Kwon, W., Looney, L. W., Mundy, L. G., Chiang, H.-F., & Kemball, A. J. 2009, ApJ, 696, 841
Lebreuilly, U., Commerçon, B., & Laibe, G. 2020, A&A, 641, A112
Lebreuilly, U., Vallucci-Goy, V., Guillet, V., Lombart, M., & Marchand, P. 2023, MNRAS, 518, 3326

Lee, C.-F., Ho, P. T. P., Li, Z.-Y., et al. 2017, NatAs, 1, 0152
Lee, C.-F., Ho, P. T. P., Palau, A., et al. 2007, ApJ, 670, 1188
Lee, C.-F., Li, Z.-Y., Hirano, N., et al. 2018, ApJ, 863, 94
Macías, E., Guerra-Alvarado, O., Carrasco-González, C., et al. 2021, A&A, 648, A33
Maret, S., Maury, A. J., Belloche, A., et al. 2020, A&A, 635, A15
Marvel, K. B., Wilking, B. A., Claussen, M. J., & Wootten, A. 2008, ApJ, 685, 285
Maury, A., Hennebelle, P., & Girart, J. M. 2022, FrASS, 9, 949223
Maury, A. J., André, P., Testi, L., et al. 2019, A&A, 621, A76
Miotello, A., Testi, L., Lodato, G., et al. 2014, A&A, 567, A32
Motte, F., & André, P. 2001, A&A, 365, 440
Natta, A., Testi, L., Calvet, N., et al. 2007, in Protostars and Planets V, ed. B. Reipurth, D. Jewitt, & K. Keil (Tucson, AZ: Univ. Arizona Press), 767
Offner, S. S. R., Moe, M., Kratter, K. M., et al. 2023, in ASP Conf. Ser. 534, Protostars and Planets VII, ed. S. Inutsuka et al. (San Francisco, CA: ASP), 275
Ohashi, N., Hayashi, M., Ho, P. T. P., & Momose, M. 1997, ApJ, 475, 211
Ormel, C. W., Paszun, D., Dominik, C., & Tielens, A. G. G. M. 2009, A&A, 502, 845
Ortiz-León, G. N., Dzib, S. A., Loinard, L., et al. 2023, A&A, 673, L1
Ortiz-León, G. N., Loinard, L., Dzib, S. A., et al. 2018a, ApJ, 865, 73
Ortiz-León, G. N., Loinard, L., Dzib, S. A., et al. 2018b, ApJL, 869, L33
Pillich, C., Bogdan, T., Landers, J., Wurm, G., & Wende, H. 2021, A&A, 652, A106
Plunkett, A. L., Arce, H. G., Corder, S. A., et al. 2015, ApJ, 803, 22
Podio, L., Codella, C., Gueth, F., et al. 2015, A&A, 581, A85
Podio, L., Codella, C., Gueth, F., et al. 2016, A&A, 593, L4
Podio, L., Tabone, B., Codella, C., et al. 2021, A&A, 648, A45
Sargent, B. A., Forrest, W. J., Tayrien, C., et al. 2009, ApJ, 690, 1193
Schilke, P., Walmsley, C. M., Pineau des Forets, G., & Flower, D. R. 1997, A&A, 321, 293
Segura-Cox, D. M., Harris, R. J., Tobin, J. J., et al. 2016, ApJL, 817, L14
Segura-Cox, D. M., Schmiedeke, A., Pineda, J. E., et al. 2020, Natur, 586, 228
Sheehan, P. D., & Eisner, J. A. 2018, ApJ, 857, 18
Silsbee, K., Akimkin, V., Ivlev, A. V., et al. 2022, ApJ, 940, 188
Tabone, B., Cabrit, S., Bianchi, E., et al. 2017, A&A, 607, L6
Tafalla, M., Santiago-García, J., Hacar, A., & Bachiller, R. 2010, A&A, 522, A91
Tazzari, M., Clarke, C. J., Testi, L., et al. 2021, MNRAS, 506, 2804
Testi, L., Birnstiel, T., Ricci, L., et al. 2014, in Protostars and Planets VI, ed. H. Beuther (Tucson, AZ: Univ. Arizona Press), 339
Trinquier, A., Elliott, T., Ulfbeck, D., et al. 2009, Sci, 324, 374
Tsukamoto, Y., Machida, M. N., & Inutsuka, S.-I. 2021, ApJL, 920, L35
Weidenschilling, S. J. 1977, MNRAS, 180, 57
Weingartner, J. C., & Draine, B. T. 2001, ApJ, 548, 296
Williams, C. D., Sanborn, M. E., Defouilloy, C., et al. 2020, PNAS, 117, 23426
Wong, Y. H. V., Hirashita, H., & Li, Z.-Y. 2016, PASJ, 68, 67
Yıldız, U. A., Kristensen, L. E., van Dishoeck, E. F., et al. 2012, A&A, 542, A86
Yoshida, T., Hsieh, T.-H., Hirano, N., & Aso, Y. 2021, ApJ, 906, 112
Ysard, N., Koehler, M., Jimenez-Serra, I., Jones, A. P., & Verstraete, L. 2019, A&A, 631, A88
Zucker, C., Speagle, J. S., Schlafly, E. F., et al. 2019, ApJ, 879, 125